A Mechanistic Picture and Kinetic Analysis of Surface-Confined Ullmann Polymerization

Marco Di Giovannantonio,[†] *Massimo Tomellini,* [$,†] *Josh Lipton-Duffin,*[@] *Gianluca Galeotti,* [‡] *Maryam Ebrahimi,* [‡] *Albano Cossaro,* [§] *Alberto Verdini,* [§] *Neerav Kharche,* [+] *Vincent Meunier,* [+] *Guillaume Vasseur,* [Ω] *Yannik Fagot-Revurat,* [¥] *Dmitrii F. Perepichka,* [∥,*] *Federico Rosei,* [‡,£,*] *Giorgio Contini*[†, #, *]

[†] Istituto di Struttura della Materia, CNR, Via Fosso del Cavaliere 100, 00133 Roma, Italy

[$] Department of Chemistry, University of Rome "Tor Vergata", Via della Ricerca Scientifica 1, 00133 Roma, Italy

[@] Institute for Future Environments, Queensland University of Technology (QUT), 2 George Street, Brisbane, QLD 4001, Australia

[‡] Centre Énergie, Matériaux et Télécommunications, Institut National de la Recherche Scientifique, 1650 Boulevard Lionel-Boulet, Varennes, QC, J3X 1S2, Canada

[+] Department of Physics, Applied Physics, and Astronomy, Rensselaer Polytechnic Institute, 110 8th Street, Troy, NY 12180, USA

[Ω] Donostia International Physics Center (DIPC), Paseo Manuel Lardizabal 4, 20018 San Sebastián, Spain

[¥] Institut Jean Lamour, UMR 7198, Université Lorraine/CNRS, B.P. 239 FE-54506, Vandoeuvre-les-Nancy, France

[§] CNR-IOM, Laboratorio TASC, 34149 Trieste, Italy

[∥] Department of Chemistry and Centre for Self-Assembled Chemical Structures, McGill University, 801 Sherbrooke Str. West, Montreal, QC H3A 2K6, Canada

[£] Institute for Fundamental and Frontier Science, University of Electronic Science and Technology of China, Chengdu, 610054, PR China.

[#] Department of Physics, University of Rome "Tor Vergata" , Via della Ricerca Scientifica 1, 00133 Roma, Italy

ABSTRACT

Surface-confined polymerization *via* Ullmann coupling is a promising route to create monolayers of one- and two-dimensional covalent π-conjugated structures, including bottom-up growth of graphene nanoribbons. Understanding the mechanism of the Ullmann reaction is needed to provide a platform for rationally controlling the formation of these materials. We use fast X-ray photoelectron spectroscopy (XPS) in kinetic measurements of epitaxial surface polymerization of 1,4-dibromobenzene on a Cu(110) surface and devise a kinetic model based on mean field rate equations, involving a transient state. This state is observed in the energy landscapes calculated by nudged elastic band (NEB) within density functional theory (DFT), which assumes as initial and

final geometries of the organometallic structure and the polymeric product those observed by scanning tunneling microscopy (STM). The kinetic model accounts for all the salient features observed in the experimental curves extracted from the fast-XPS measurements and enables an enhanced understanding of the polymerization process, that is found to follow a nucleation-and-growth behavior preceded by the formation of a transient state.

INTRODUCTION

The formation of extended covalent surface-confined molecular structures is an exciting scientific challenge and technological prospect. Reaction pathways leading to novel low-dimensional systems have been identified in a variety of different environments, and a number of reviews summarizing the state-of-the-art have been published recently.[1-8] Reactions have been performed at the solid-liquid interface *via* external *stimuli* such as voltage pulses from the tip of a scanning probe microscope,[9] by UV light,[10-11] and by varying the electrochemical redox potential[12-14] or the pH of the solution.[15-17] In ambient conditions condensation reactions have led to the formation of covalent organic frameworks by thermal activation.[18-19] A variety of reactions producing both 1D[20-24] and 2D[25-28] polymers have been studied on metal surfaces in ultra-high vacuum (UHV) conditions, with the aim of creating graphene-like nanostructures.[29-31] The most popular approach is based on Ullmann coupling, a metal-catalyzed coupling reaction between aryl halides[32] which allows to precisely select the active sites of the molecules upon introduction of halogen atoms in these positions, and build the desired nanostructure from a rationally designed building block.[20, 22, 24-25, 33-37] This method is also adopted as a first synthesis step in the on-surface growth of graphene nanoribbons, before the cyclodehydrogenation process.[29, 31, 38] However, Ullmann coupling has so far demonstrated a limited ability to create large ordered domains of extended conjugated networks, which would be necessary for deployment of these materials into device applications. The mechanistic picture of the reaction pathways given in this study provides a framework for understanding the present limitations, which will ultimately be necessary in charting a route towards the controlled formation of ordered (*i.e.,* defect-free continuous networks) and long-range conjugated polymeric domains to be implemented in technological applications.

Ullmann polymerization proceeds via two steps: (i) dehalogenation of the precursor molecule, which results in the immediate formation of an organometallic intermediate, followed by (ii) ejection of the interstitial metal atom to form a C–C bond between building blocks.[23, 39-40] The barriers to each of these steps are governed by substrate reactivity, and in general are anti-correlated.[34] On surfaces where the barrier to dehalogenation is large (*e.g.,* Au(111)), the barrier for ejecting the interstitial metal centers is often so low that the second step proceeds immediately, and the organometallic state is seldom observed. Conversely, on surfaces where the barrier to dehalogenation is low (*e.g.,* Cu(110)), considerable heating above room temperature (RT) is required to convert the intermediate state to a polymer. The internal periodicity of these organometallics is necessarily different from that of the corresponding polymers, due to the incorporation of additional metal atoms between the molecular building blocks. As such, the

arrangement of the organometallic phase with respect to the substrate is expected to be different than that of the polymer phase, as the smaller polymer lattice constant will drive the overlayer into a new orientation to satisfy substrate commensurability. This has been clearly observed both for 1D[20-21, 24] and 2D[26, 41] topologies.

Developing a full understanding of Ullmann coupling has been the focus of many surface scientists over the past two decades.[42-44] Most recently, a number of studies have addressed the kinetics of this coupling process using Monte Carlo simulations to model molecular surface diffusion.[33-34, 45] These simulations start with a seed molecule fixed at a given position on a surface, and other molecules that randomly walk until reaching a site adjacent to the seed (reactive site), where they can either couple to the seed (irreversible process) or back-diffuse (exploiting the reversibility typical of supramolecular interactions). The coupling probability (P) is therefore defined as:

$$P = \frac{\nu_c}{\nu_c + \nu_d} \tag{1}$$

where ν_c and ν_d are the probabilities per unit time of the two complementary processes of coupling and back-diffusion, respectively. Monte Carlo simulations show that for $P \sim 1$ (*i.e.*, coupling is the more favorable mechanism) fractal-like polymer structures are obtained, while for $P \ll 1$ (*i.e.*, back-diffusion is more favorable) domains ordered over a long range are formed on the surface. These simulations qualitatively match the morphologies observed by scanning tunneling microscopy (STM) of polymers obtained by use of different molecule/surface combinations, and thereby provide an indication that this type of model is able to capture salient features of Ullmann polymerization in two-dimensions.[33, 45] However, the Monte Carlo approach described above only provides a qualitative picture, affording no quantitative insight into the energetics of the coupling reaction, nor the time dependent yield of polymerization from the organometallic phase.

Here we apply a more comprehensive kinetic approach which exploits a microscopic picture of the polymerization process. In particular, we adopt a kinetic scheme usually employed for polymerization in solution,[46] which considers initiation and elongation, and also takes into account surface diffusion of monomers, which is a fundamental process for reactions on solid surfaces.[47] Our approach differs from both polymerization in solution and reactions on solid surfaces via vapor deposition in some aspects. Since no additional phenyl groups are added to the surface during the reaction, the system under investigation is closed. This condition is taken into account in our model, whereby no flux of incoming monomers appears in the system of rate equations. Moreover, the polymerization reaction is known to be irreversible, so the model excludes any reverse reaction once the polymers are formed, in agreement with experimental evidences[20, 24-25, 33, 35-37] and potential energy curves obtained by DFT[34] (also confirmed by our results).

This work explores the kinetics of on-surface Ullmann polymerization, making direct use of experimental data showing the transition from the organometallic to the polymeric phase.[20] We explored the formation of a model π-conjugated polymer (poly(*para*-phenylene), PPP) from 1,4-dibromobenzene (dBB), by monitoring the process with fast X-ray photoelectron spectroscopy (fast-XPS) which has both sufficient chemical sensitivity to monitor the reaction, and sufficient time resolution to observe the kinetics in real-time. Density functional theory (DFT) calculations predict the presence of a transient before the intermolecular coupling, on the basis of which we propose a kinetic model that reproduces the experimental data obtained from fast-XPS measurements and thus provides an important insight into the polymerization mechanism.

RESULTS AND DISCUSSION

STM and fast-XPS data

The polymerization of dBB on Cu(110) is described in Scheme 1. The RT deposition of dBB on the surface results in the complete dehalogenation of the molecules. Figure 1a shows STM images of a similar low-coverage phase observed on the same surface, described in our previous work.[20] A tentative model is sketched in the insets of Figure 1a and b. The bright features are assigned to metal bridges,[48-50] linking to phenylene building blocks to form a chain-like structure. The dimmer features are likely to be bromine atoms. The detailed nature of this structure will be the topic of a future publication. Upon heating of the substrate, the metal atoms are ejected and the building blocks couple to each other *via* covalent bonding, as shown in our previous works.[20-21, 23-24] The resulting polymeric phase is shown in the STM image of Figure 1b where chains of 1D polymers are alternated with rows of bromine atoms. The unit cell (indicated by dashed lines) contains three phenylene units for the organometallic phase (Figure 1a) and one unit in the polymer chains (Figure 1b). The transition between these two phases (organometallic intermediate and polymer) is accompanied by a change in the orientation of their longitudinal axis from 41° to 54° with respect to the [1$\bar{1}$0] direction.
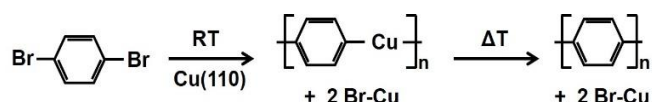
**Scheme 1.** Reaction scheme of 1,4-dibromobenzene (dBB) undergoing Ullmann coupling on Cu(110).
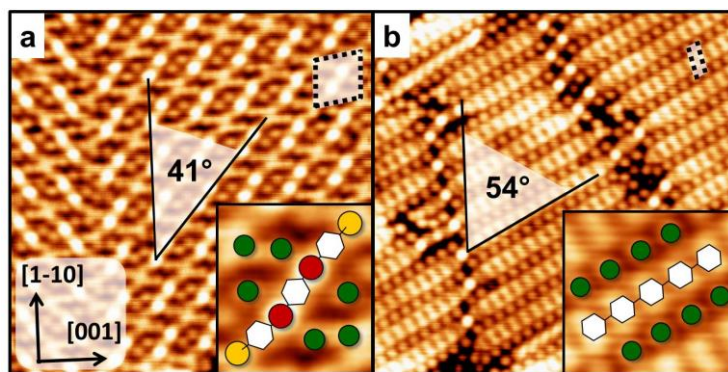
Figure 1. STM images (11.5×11.5 nm^2, I$_t$=0.5 nA, V$_b$=20 mV) acquired in constant current mode at a substrate temperature of 5 K of (a) a saturated monolayer of dBB deposited at RT on Cu(110), forming an ordered assembly of organometallic units, and (b) after annealing to 500 K obtaining 1D polymers. The epitaxy matrices are (1, -4 | 6, 0) and (1, -1 | 4, 1), respectively (black dashed lines). Insets report drawings of the structures assigned to the RT (a) and annealed (b) phases. White hexagons and green circles represent phenylene units and Br atoms, respectively. Yellow and red circles represent copper atoms linked respectively to one or two phenylene units (the latter appearing as higher protrusion in the STM imaging).

The transformation of the organometallic phase into polymers was monitored as a function of temperature by fast-XPS measurements of the C 1s core level. Figure 2 (top panels) shows fast-XPS results from separate experiments using different heating rates. A change in the C 1s spectrum provides a signature for the transition from the organometallic (reactants, formed instantaneously upon depositing the molecules on the surface at RT) to the polymer (products), with peak maxima at binding energies of 283.8 eV and 284.5 eV, respectively.[20-21] Kinetic curves representing the normalized surface density of reactant molecules as a function of temperature were extracted from the fast-XPS data, following a procedure described in the Supporting Information, and are shown in the bottom panel of Figure 2. A change in the onset of the reaction is observed with different heating rates, reflecting the non-equilibrium nature of the observed transition, with the composition of the surface controlled not only by temperature but also by reaction time (kinetics). As shown above this transition is accompanied by a change in the orientation of the organometallic and polymeric phases, implying a diffusion of the precursors during the polymerization reaction, which will be taken into account in the modeling reported below.
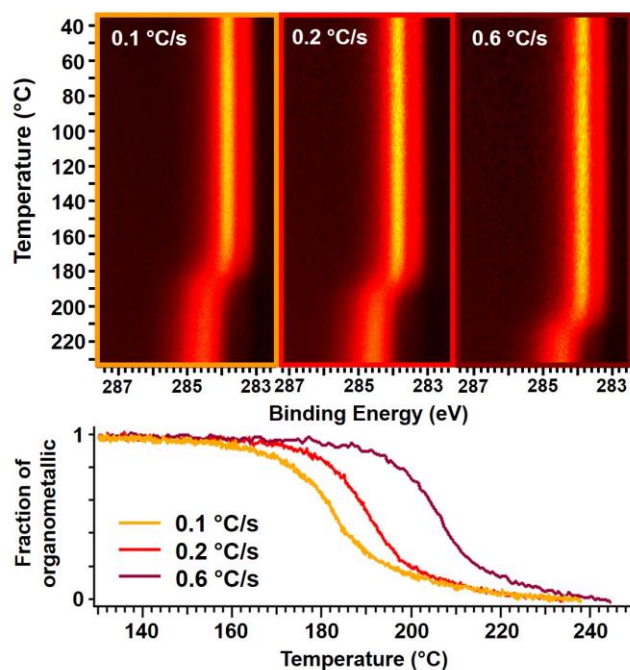
Figure 2. Top: fast-XPS maps for the C 1s core level signals of dBB deposited on Cu(110) and annealed using three different heating rates: 0.1 ℃/s, 0.2 ℃/s and 0.6 ℃/s. Bottom: kinetic curves extracted from the fast-XPS maps, as described in the Supporting Information. These curves represent the normalized surface density of reactant molecules present on the surface in the organometallic phase as a function of the temperature.

Density functional theory calculations: potential energy curves

DFT calculations were performed to explore the transformation from organometallic to polymer phases by investigating the diffusion of phenyl building blocks on the copper surface (we identify these units as 'monomers') and their coupling into polymer chains. Two steps of the polymerization process were modeled: the coupling of two monomers into a dimer, and the addition of a monomer to an existing dimer to form a trimer. The initial orientation of the monomers was fixed according to the STM image of Figure 1a, *i.e.,* with the axis connecting the two C-Cu bonds of the monomer along $[1\bar{1}\bar{1}]$, while the dimer and the trimer orientations were imposed as that of the polymers observed in Figure 1b, *i.e.* along $[1\bar{1}\bar{2}]$. As discussed above, the transition must involve a diffusion of the molecular species. Calculations show the diffusion to be most favorable along the $[1\bar{1}0]$ direction (energy barrier of 0.39 eV), as shown in Figure 3. Along this direction the energy potential curve exhibits a shallow local minimum at about 1.5 Å located between the positions of the two more stable configurations of the monomer, representing a transient species for the diffusion process.
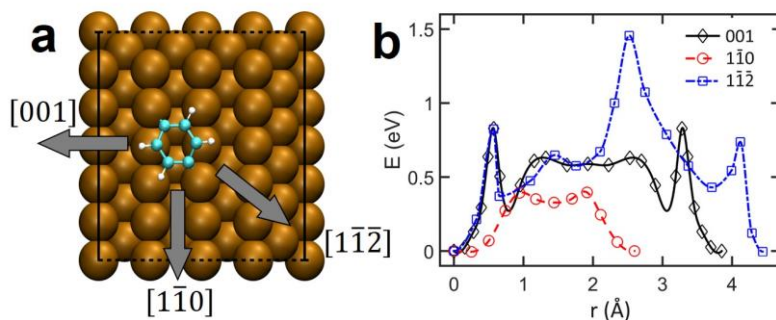
Figure 3. DFT calculations for the diffusion barriers of one monomer along three high-symmetry directions of the Cu(110) surface. The diffusion along the $[1\bar{1}0]$ direction has the lowest activation barrier (0.39 eV).

The diffusion and coupling of two isolated monomers can be described by a total energy landscape, in terms of the monomers' center-to-center distance (Figure 4a). When sufficiently separated (r > 7 Å, Figure 4b, grey arrow in Figure 4a), the two monomers are most likely to diffuse along the $[1\bar{1}0]$ direction. As the two monomers approach one another they may bind to the same copper atom of the substrate (Figure 4c), which, as a result, is partially pulled out of the surface plane (side views of the structures are shown in Figure S2b in Supporting Information). This configuration corresponds to a local minimum in the potential energy curve (orange arrow in Figure 4a) which is more stable than isolated monomers, and corresponds to the formation of the experimentally observed organometallic phase.[20, 24] The presence of this minimum is corroborated by the fact that isolated monomers are never observed by STM imaging (even when the surface is subsequently cooled to 4 K after deposition), implying that organometallic coupling between monomers is favored at RT. When the temperature is increased, the shared copper atom can be ejected, leading the monomers to bind covalently. When the distance between the rings is approximately 6 Å, the system reaches a configuration that we refer to as the transient state (Figure 4d, corresponding to the green arrow in Figure 4a, and Figure S2c in Supporting Information). From this configuration the monomers may either couple to form a dimer (overcoming the barrier E_2) or back-diffuse to the stable organometallic phase (barrier E_{-1}) as two competing kinetic processes. A local minimum is also observed for the trimerization process (green arrow in Figure 4f). This represents again the transient configuration (Figure 4h and Figure S2f in Supporting Information) from which the system can evolve by forming a trimer (overcoming the barrier E_3) or by back-diffusion of the monomer (overcoming barrier E_{-1}) as competing processes. In the case of trimerization, we could not identify in the DFT simulations any local minimum with energy lower than the initial one. This is perhaps unsurprising in this model, as the participating phenyl in a dimer (or higher-order oligomers) is situated above the substrate hollow site, whereas free monomers prefer the long-bridge site. Thus the positioning of building blocks with respect to the substrate atoms is the same

for all additions of monomers to a dimer (or longer chain), but is different for creation of a dimer from individual monomers. At the beginning of the two potential energy curves local minima at about 7.5 Å (Figure 4a) and 6.5 Å (Figure 4f) can be observed: these are related to monomer diffusion along the $[1\bar{1}0]$ direction, as observed in Figure 3b. The energy barriers involved in the coupling processes are reported in Table 1. Animations showing all the steps of the coupling are available in the Supporting Information. The activation energy for dimerization is higher than that for trimerization. This is related to the higher value of E_1 in the first case, due to the presence of the highly stable assembly of the organometallic phase, which is missing in case of the growth of a polymeric chain.
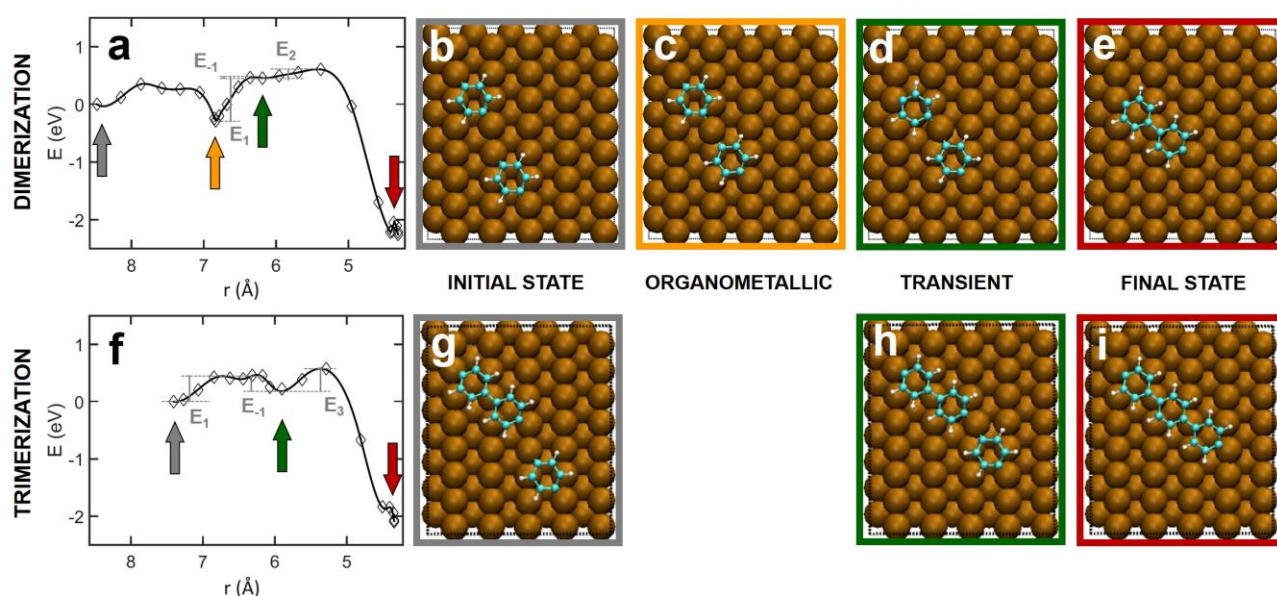

Figure 4. a, f: coupling barriers between two monomers (dimerization) or a monomer and a dimer (trimerization), respectively. The length (r) indicated in angstrom is the distance between the centers of the aromatic rings which undergo covalent coupling. The geometries of the most significant states (initial, organometallic intermediate, transient and final) are reported in panels b-e and in panels g-i for the dimerization and trimerization, respectively. The colors of the frames correspond to the arrows in panels a and f.

Table 1. Energy barriers obtained from DFT calculations: E_1 is the transformation of the monomer into a transient, E_{-1} is its back-diffusion, E_2 and E_3 are the dimerization and trimerization barriers, respectively. E_n and E_g indicate the nucleation and growth activation energies, respectively, with $E_n = E_1 - E_{-1} + E_2$ and $E_g = E_1 - E_{-1} + E_3$ (see the following section Kinetic model). All the energies are expressed in eV.

	E_1	E_{-1}	E_2 and E_3	E_n	E_g
Dimerization	0.75	0.01	0.15	0.89	---
Trimerization	0.43	0.23	0.35	---	0.55

Kinetic model

Using the shape of the curves in Figure 2 it is now possible to comment on the kinetic order of the reaction. A completely ordered *topotactic*[51-53] transformation of the organometallic to polymer should ideally follow zero-order reaction kinetics: $\frac{dn_1}{dt} = -k$, where n_1 is the surface density of phenylene units in the organometallic phase, and k is the temperature dependent rate constant. In this scenario the growing polymer chain has always a next neighbor monomer available for coupling and surface density has no bearing on the rate equation. A characteristic feature of zero-order kinetics is that polymerization reaches completion with a non-zero rate. This is clearly not the case for the curves shown in Figure 2. Instead, the progressively decreasing reaction rate observed near completion of the reaction is a hallmark of a diffusion-controlled process. To account for this behavior, the surface density of the phenylene units must be taken into account in the kinetic model. This brought us to model the system by a phenomenological kinetic approach, using one kinetic rate equation of order m (Section 7.2 in Supporting Information), but the quality of the resulting fit is not satisfactory. Therefore, exploiting the results obtained from our DFT calculations and hypotheses made in prior works using Monte Carlo simulations,[33-34, 45] we develop an approach based on a system of mean field rate equations which describes the key processes during polymer formation: (i) coupling between monomers to produce dimers, and (ii) growth of polymeric aggregates through monomer addition. In this work the surface density of monomers and its evolution in temperature are quantified *via* the fast-XPS measurements. We explicitly account for the formation of a transient state (suggested in the DFT analysis) that mediates dimer and polymer formation (Scheme 2). The presence of this state also arises from the definition of the probability (P) introduced in the Monte Carlo approach which implies coupling and back-jump diffusion as two competing processes (see Section 5 of Supporting Information for further discussion). The addition of a monomer to an existing chain (two units or longer) is considered energetically inequivalent to dimerization, because of the different species involved in the coupling and the potential energy landscapes derived from the DFT calculations above. The surface density of halogens (byproduct of the dehalogenation reaction after RT adsorption of dBB on Cu(110)) is not directly taken into account in the kinetic model, although their effect enters implicitly in the rate constants. The halogen diffusion rate is much higher than that of the monomers (Figure S3 in Supporting Information).
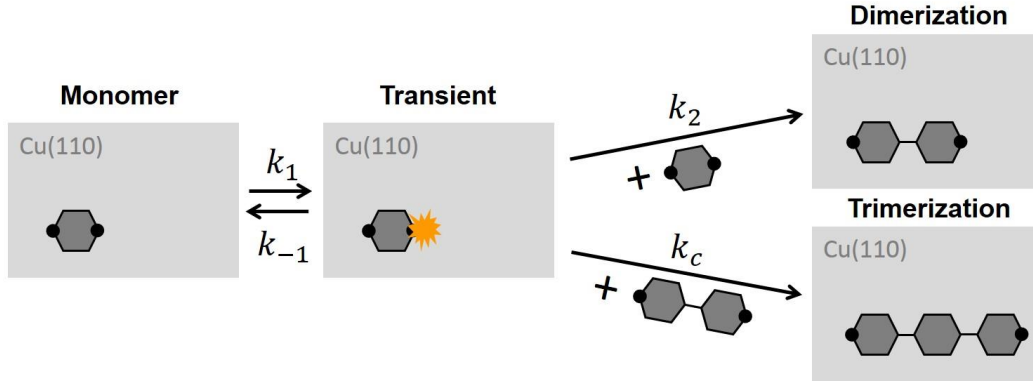
Scheme 2. Proposed kinetic model described by kinetic equation (2).

Based on the above discussion, the mean field rate equations of the kinetic model can be written as follows:

$$
\begin{cases}
\frac{dn_1^*}{dt} = k_1\, n_1 - n_1^*(k_{-1} + k_2\, n_1 + k_c\, N) \\
\frac{dN}{dt} = k_2\, n_1 n_1^* \\
\frac{dn_1}{dt} = -k_1\, n_1 + n_1^*(k_{-1} - k_2\, n_1)
\end{cases}
\tag{2}
$$

were n_1 and n_1^* are the surface densities of free monomers and monomers in the transient state, respectively. N is the surface density of stable aggregates on the surface, *i.e.,* chains made up of a number of monomers greater than or equal to 2: $N = \sum_{i \geq 2} n_i$ where n_i is the surface density of polymer chains with i monomers. k_1 and k_{-1} are first order rate constants for the formation of the transient and its back-transformation, respectively, while k_2 and k_c are second order rate constants for dimerization and the addition of a monomer to a longer chain, respectively.

The transient state is short-lived and its surface density is low. This allows the use of the steady state approximation, *i.e.* we may set $\frac{dn_1^*}{dt} \cong 0$ and assert that n_1^* is small compared to the other species ($n_1^* \ll n_1$). The first equation in (2) becomes $n_1^* \cong n_1 \left[\frac{k_1}{k_{-1}+k_2\, n_1+k_c\, N}\right]$ and since $n_1^* \ll n_1$, we know $\frac{k_1}{k_{-1}+k_2\, n_1+k_c\, N} \ll 1$. The system of equations (2) reduces to:

$$
\begin{cases}
\frac{dN}{dt} = \frac{k_1\, k_2\, n_1^2}{k_{-1}+k_2\, n_1+k_c\, N} \\
\frac{dn_1}{dt} = -k_1\, n_1 + \frac{k_1\, n_1(k_{-1}-k_2\, n_1)}{k_{-1}+k_2\, n_1+k_c\, N}
\end{cases}
\tag{3}
$$

The condition that $\frac{k_1}{k_{-1}+k_2\,n_1+k_c\,N} \ll 1$ can be fulfilled in three distinct cases, corresponding to different energy barriers for the polymerization process, as sketched in Figure 5. For case (i) (k_{-1} greater than $k_2\,n_1$, $k_c\,N$ and k_1), transients are more likely to back-diffuse and remain as monomers rather than couple to neighbors ($P \ll 1$). For both cases (ii) ($k_2\,n_1$ greater than k_{-1}, $k_c\,N$ and k_1) and (iii) ($k_2\,n_1$ greater than k_{-1} and k_1) coupling is more probable ($P\sim1$). However, case (ii) favors dimerization only, whereas case (iii) favors any type of coupling. The system of coupled first-order differential equations is reduced to a single second order non-linear differential equation for the normalized density of monomers $n_1/n_1(0)$, where $n_1(0)$ is the density of monomers in the organometallic state at the start of the experiment. The equation is solved numerically and the activation energies for nucleation and growth (E_n and E_g, respectively) can be extracted by fitting the solution of the equation to the experimental kinetic curves extracted from the fast-XPS experiments.
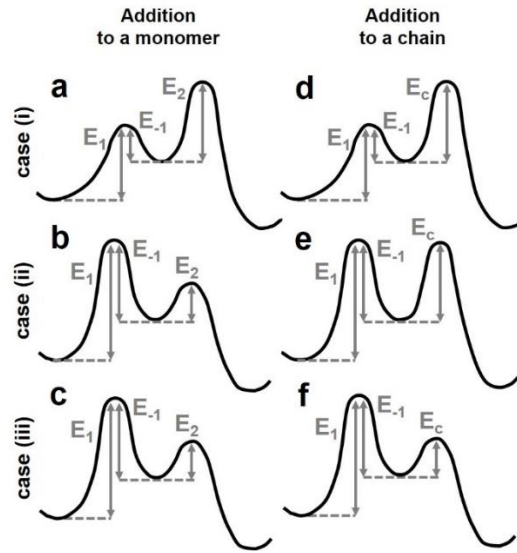
Figure 5. Energy barriers for the possible interactions of the species present on the surface in the three cases: (i) k_{-1} greater than $k_2\,n_1$, $k_c\,N$ and k_1, (ii) $k_2\,n_1$ greater than k_{-1}, $k_c\,N$ and k_1, and (iii) $k_2\,n_1$ greater than k_{-1} and k_1. The cases involving the formation of dimers or the addition of a monomer to a pre-existing polymeric chain (growth of a polymer) are reported on the left and right side, respectively. E_1 and E_{-1} are the energy barriers for the formation and disappearance of the transient, E_2 for the dimerization and E_c for the addition of a monomer to a longer chain.
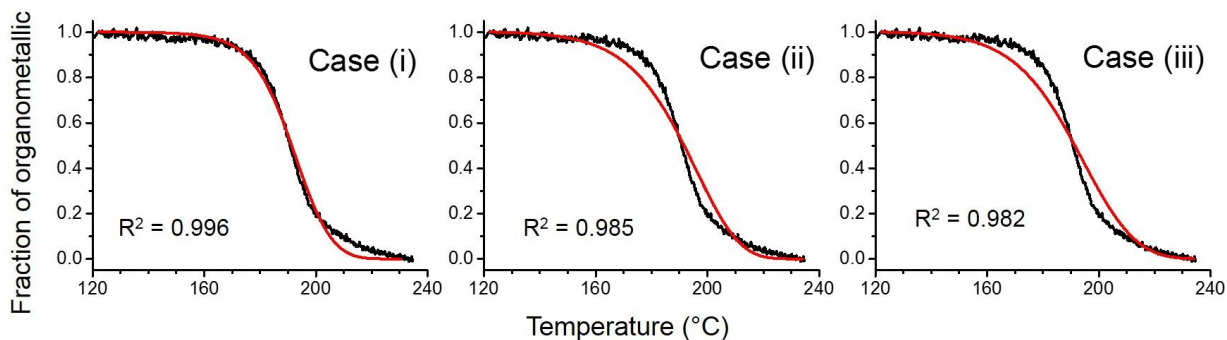
Figure 6. Comparison between the fit (red curves) of an experimental kinetic curve (in black, for dBB/Cu(110) annealed at 0.2 °C/s) performed for each of the cases described above. The first limiting case of the kinetic model best fits the experimental data.

Figure 6 shows that the best fit is obtained for case (i) (k_{-1} is the dominant term), where coupling is less likely than back-diffusion. For this case equations (3) simplify to (see Section 7.1 in Supporting Information):

$$\begin{cases} \frac{d\eta}{dT} = \frac{1}{\phi} \frac{k_1 \tilde{k}_2}{k_{-1}} x_1^2 \\ \frac{dx_1}{dT} = -\frac{1}{\phi} \left[2 \frac{k_1 \tilde{k}_2}{k_{-1}} x_1^2 + \frac{k_1 \tilde{k}_c}{k_{-1}} \eta x_1 \right] \end{cases} \tag{4}$$

where, $\phi = \frac{dT}{dt}$ is the heating rate, $\tilde{k}_2 = n_1(0)k_2$, $\tilde{k}_c = n_1(0)k_c$, $\eta = \frac{N}{n_1(0)}$ and $x_1 = \frac{n_1}{n_1(0)}$.

The system of equations (4) is equivalent to the one usually employed for modeling nucleation and growth of thin films.[47, 54] Setting $k_n = \frac{k_1 \tilde{k}_2}{k_{-1}}$ and $k_g = \frac{k_1 \tilde{k}_c}{k_{-1}}$ in equations (4) allows us to define effective rate coefficients for nucleation (dimer formation) and growth with activation energies given respectively by $E_n = E_1 + E_2 - E_{-1}$ and $E_g = E_1 + E_c - E_{-1}$.[47, 54] The full mathematical approaches describing in detail all discussed cases and the final differential equations used to fit the data are reported in Section 7 of the Supporting Information.

From the fit for case (i) we find values for the activation barriers for the nucleation (dimerization) and growth to be 1.310±0.005 eV and 1.090±0.005 eV, respectively (Figure S5 in the Supporting Information). The extracted activation barriers do not depend on the heating rate, thereby supporting the validity of the model. While the absolute values of the experimental activation barriers are systematically higher than those calculated by DFT, our findings do support the hypothesis that the barrier for nucleation is larger than the barrier for growth, owing to the stability of organometallic structure. It should be noted that even in case (i), where the model best fits the experimental kinetics, there is a slight deviation of the two curves as the reaction completes

13

(Figure 6). This may arise from the increasing spatial extent of the polymers, which hinder the free diffusion of monomers and thereby add a coverage-dependence to the rate constant that is not taken into account in the present model. Our results for the energy barriers and pre-exponential factors are comparable to those experimentally determined by temperature programmed reaction experiments for biphenyl formed from halobenzenes on Cu(111): in that work the activation energies and pre-exponential factors range from 0.9 to 1.5 eV and from 6×10^{11} to $7 \times 10^{15} s^{-1}$ respectively.[42]

CONCLUSIONS AND PERSPECTIVES

Kinetic analysis of surface-confined Ullmann polymerization of 1,4-dibromobenzene using fast-XPS data and DFT calculations has enabled the development of a mechanistic picture of the reaction, which postulates the presence of a transient state during the reaction. From this conceptualization a kinetic model incorporating a nucleation and growth mechanism is able to describe the experimental kinetics when using differing heating rates. The experimental fast-XPS data is most accurately described by a scenario where coupling probability between the monomers is low, in agreement with STM observations of domains composed of long polymers. Both the DFT calculations and the kinetic model suggest that the energy barrier for nucleation is larger than the barrier for growth. This is consistent with the presence of stable assemblies of monomers in the organometallic phase at RT. Growth of a polymer from an existing nucleus (dimer) requires substantially less energy than creating the nucleus out of the stable RT phase.

The combination of experimentally measured kinetic curves, DFT calculations and kinetic modelling offers new insight into the mechanistic process of surface-confined Ullmann coupling. Our results suggest that the polymerization reaction is not *topotactic*, but rather a diffusion-controlled process. The methodology here reported can be applied to other systems/reactions to extend the understanding of the mechanics surface-confined chemistry.

ASSOCIATED CONTENT

Supporting Information

The Supporting Information is available free of charge on the ACS Publications website at DOI: …
    Experimental details, computational details, method for extracting kinetic curves from fast-XPS maps, side views of the molecular geometries calculated by DFT, coupling probability (P) and kinetics: the transient species, diffusion of the bromine, full mathematical approaches for the kinetic models, kinetic curves obtained for different heating rates and the absolute energies

and coordinates of the atoms for optimized geometries (PDF). Side and top views of the trajectories for dimerization and trimerization coupling (AVI).

AUTHOR INFORMATION

Corresponding Authors

* dmitrii.perepichka@mcgill.ca; rosei@emt.inrs.ca; giorgio.contini@cnr.it

Notes

The authors declare no competing financial interest.

ACKNOWLEDGMENTS

REFERENCES

(1)   El Garah, M.; MacLeod, J. M.; Rosei, F. *Surf. Sci.* **2013,** *613*, 6-14.

(2)   Lindner, R.; Kühnle, A. *Chem. Phys. Chem.* **2015,** *16*, 1582-1592.

(3)   Dong, L.; Liu, P. N.; Lin, N. *Acc. Chem. Res.* **2015,** *48*, 2765-2774.

(4)   Gourdon, A. *Angew. Chem. Int. Edit.* **2008,** *47*, 6950-6953.

(5)   Perepichka, D. F.; Rosei, F. *Science* **2009,** *323*, 216-217.

(6)   Lackinger, M.; Heckl, W. M. *J. Phys. D Appl. Phys.* **2011,** *44*, 464011.

(7)   Sakamoto, J.; van Heijst, J.; Lukin, O.; Schlüter, A. D. *Angew. Chem. Int. Edit.* **2009,** *48*, 1030-1069.

(8)   Franc, G.; Gourdon, A. *Phys. Chem. Chem. Phys.* **2011,** *13*, 14283-14292.

(9)   Okawa, Y.; Aono, M. *Nature* **2001,** *409*, 683-684.

(10) Grim, P. C. M.; De Feyter, S.; Gesquière, A.; Vanoppen, P.; Rüker, M.; Valiyaveettil, S.; Moessner, G.; Müllen, K.; De Schryver, F. C. *Angew. Chem. Int. Edit. Engl.* **1997,** *36*, 2601-2603.

(11) Miura, A.; De Feyter, S.; Abdel-Mottaleb, M. M. S.; Gesquière, A.; Grim, P. C. M.; Moessner, G.; Sieffert, M.; Klapper, M.; Müllen, K.; De Schryver, F. C. *Langmuir* **2003,** *19*, 6474-6482.

(12) Yau, S.; Lee, Y.; Chang, C.; Fan, L.; Yang, Y.; Dow, W.-P. *J. Phys. Chem. C* **2009,** *113*, 13758-13764.

(13) Sakaguchi, H.; Matsumura, H.; Gong, H.; Abouelwafa, A. M. *Science* **2005,** *310*, 1002-1006.

(14) Sakaguchi, H.; Matsumura, H.; Gong, H. *Nat. Mater.* **2004,** *3*, 551-557.

(15) Tanoue, R.; Higuchi, R.; Enoki, N.; Miyasato, Y.; Uemura, S.; Kimizuka, N.; Stieg, A. Z.; Gimzewski, J. K.; Kunitake, M. *ACS Nano* **2011,** *5*, 3923-3929.

(16) Di Giovannantonio, M.; Kosmala, T.; Bonanni, B.; Serrano, G.; Zema, N.; Turchini, S.; Catone, D.; Wandelt, K.; Pasini, D.; Contini, G.; Goletti, C. *J. Phys. Chem. C* **2015,** *119*, 19228-19235.

(17) Ciesielski, A.; El Garah, M.; Haar, S.; Kovaříček, P.; Lehn, J.-M.; Samorì, P. *Nat. Chem.* **2014,** *6*, 1017-1023.

(18) Dienstmaier, J. F.; Gigler, A. M.; Goetz, A. J.; Knochel, P.; Bein, T.; Lyapin, A.; Reichlmaier, S.; Heckl, W. M.; Lackinger, M. *ACS Nano* **2011,** *5*, 9737-9745.

(19) Liu, X.-H.; Guan, C.-Z.; Ding, S.-Y.; Wang, W.; Yan, H.-J.; Wang, D.; Wan, L.-J. *J. Am. Chem. Soc.* **2013,** *135*, 10470-10474.

(20) Di Giovannantonio, M.; El Garah, M.; Lipton-Duffin, J.; Meunier, V.; Cardenas, L.; Fagot Revurat, Y.; Cossaro, A.; Verdini, A.; Perepichka, D. F.; Rosei, F.; Contini, G. *ACS Nano* **2013,** *7*, 8190-8198.

(21) Di Giovannantonio, M.; El Garah, M.; Lipton-Duffin, J.; Meunier, V.; Cardenas, L.; Fagot-Revurat, Y.; Cossaro, A.; Verdini, A.; Perepichka, D. F.; Rosei, F.; Contini, G. *ACS Nano* **2014,** *8*, 1969-1971.

(22) Lafferentz, L.; Ample, F.; Yu, H.; Hecht, S.; Joachim, C.; Grill, L. *Science* **2009,** *323*, 1193-1197.

(23) Lipton-Duffin, J. A.; Ivasenko, O.; Perepichka, D. F.; Rosei, F. *Small* **2009,** *5*, 592-597.

(24) Vasseur, G.; Fagot-Revurat, Y.; Sicot, M.; Kierren, B.; Moreau, L.; Malterre, D.; Cardenas, L.; Galeotti, G.; Lipton-Duffin, J.; Rosei, F.; Di Giovannantonio, M.; Contini, G.; Le Fevre, P.; Bertran, F.; Liang, L.; Meunier, V.; Perepichka, D. F. *Nat. Commun.* **2016,** *7*, 10235.

(25) Grill, L.; Dyer, M.; Lafferentz, L.; Persson, M.; Peters, M. V.; Hecht, S. *Nat. Nano.* **2007,** *2*, 687-691.

(26) Gutzler, R.; Walch, H.; Eder, G.; Kloft, S.; Heckl, W. M.; Lackinger, M. *Chem. Commun.* **2009,** 4456-4458.

(27) Haq, S.; Hanke, F.; Sharp, J.; Persson, M.; Amabilino, D. B.; Raval, R. *ACS Nano* **2014,** *8*, 8856-8870.

(28) Zwaneveld, N. A. A.; Pawlak, R. m.; Abel, M.; Catalin, D.; Gigmes, D.; Bertin, D.; Porte, L. *J. Am. Chem. Soc.* **2008,** *130*, 6678-6679.

(29) Cai, J.; Ruffieux, P.; Jaafar, R.; Bieri, M.; Braun, T.; Blankenburg, S.; Muoth, M.; Seitsonen, A. P.; Saleh, M.; Feng, X.; Mullen, K.; Fasel, R. *Nature* **2010,** *466*, 470-473.

(30) Han, P.; Akagi, K.; Federici Canova, F.; Mutoh, H.; Shiraki, S.; Iwaya, K.; Weiss, P. S.; Asao, N.; Hitosugi, T. *ACS Nano* **2014,** *8*, 9181-9187.

(31) Basagni, A.; Sedona, F.; Pignedoli, C. A.; Cattelan, M.; Nicolas, L.; Casarin, M.; Sambi, M. *J. Am. Chem. Soc.* **2015,** *137*, 1802-1808.

(32) Ullmann, F.; Bielecki, J. *Ber. Deut. Chem. Ges.* **1901,** *34*, 2174-2185.

(33) Bieri, M.; Nguyen, M.-T.; Groning, O.; Cai, J.; Treier, M.; Ait-Mansour, K.; Ruffieux, P.; Pignedoli, C. A.; Passerone, D.; Kastler, M.; Mullen, K.; Fasel, R. *J. Am. Chem. Soc.* **2010,** *132*, 16669-16676.

(34) Björk, J.; Hanke, F.; Stafström, S. *J. Am. Chem. Soc.* **2013,** *135*, 5768-5775.

(35) Bombis, C.; Ample, F.; Lafferentz, L.; Yu, H.; Hecht, S.; Joachim, C.; Grill, L. *Angew. Chem. Int. Edit.* **2009,** *48*, 9966-9970.

(36) Gutzler, R.; Fu, C.; Dadvand, A.; Hua, Y.; MacLeod, J. M.; Rosei, F.; Perepichka, D. F. *Nanoscale* **2012,** *4*, 5965-5971.

(37) Wang, W.; Shi, X.; Wang, S.; Van Hove, M. A.; Lin, N. *J. Am. Chem. Soc.* **2011,** *133*, 13264-13267.

(38) de Oteyza, D. G.; García-Lekue, A.; Vilas-Varela, M.; Merino-Díez, N.; Carbonell-Sanromà, E.; Corso, M.; Vasseur, G.; Rogero, C.; Guitián, E.; Pascual, J. I.; Ortega, J. E.; Wakayama, Y.; Peña, D. *ACS Nano* **2016,** *10*, 9000-9008.

(39) McCarty, G. S.; Weiss, P. S. *J. Am. Chem. Soc.* **2004,** *126*, 16772-16776.

(40) Björk, J. *J. Phys.: Condens. Matter* **2016,** *28*, 083002.

(41) Cardenas, L.; Gutzler, R.; Lipton-Duffin, J.; Fu, C.; Brusso, J. L.; Dinca, L. E.; Vondracek, M.; Fagot-Revurat, Y.; Malterre, D.; Rosei, F.; Perepichka, D. F. *Chem. Sci.* **2013,** *4*, 3263-3268.

(42) Meyers, J. M.; Gellman, A. J. *Surf. Sci.* **1995,** *337*, 40-50.

(43) Xi, M.; Bent, B. E. *Surf. Sci.* **1992,** *278*, 19-32.

(44) Xi, M.; Bent, B. E. *J. Am. Chem. Soc.* **1993,** *115*, 7426-7433.

(45) Eichhorn, J.; Nieckarz, D.; Ochs, O.; Samanta, D.; Schmittel, M.; Szabelski, P. J.; Lackinger, M. *ACS Nano* **2014,** *8*, 7880-7889.

(46) Bishop, M. F.; Ferrone, F. A. *Biophys. J.* **1984,** *46*, 631-644.

(47) Brune, H. *Surf. Sci. Rep.* **1998,** *31*, 125-229.

(48) Eichhorn, J.; Strunskus, T.; Rastgoo-Lahrood, A.; Samanta, D.; Schmittel, M.; Lackinger, M. *Chem. Commun.* **2014,** *50*, 7680-7682.

(49) Lewis, E. A.; Murphy, C. J.; Liriano, M. L.; Sykes, E. C. H. *Chem. Commun.* **2014,** *50*, 1006-1008.

(50) Saywell, A.; Greń, W.; Franc, G.; Gourdon, A.; Bouju, X.; Grill, L. *J. Phys. Chem. C* **2014,** *118*, 1719-1728.

(51) Vogg, G.; Brandt, M. S.; Stutzmann, M. *Chem. Mater.* **2003,** *15*, 910-915.

(52) Ando, D. J.; Bloor, D.; Tieke, B. *Macromol. Chem., Rapid. Commun.* **1980,** *1*, 385-388.

(53) Kollmar, C.; Sixl, H. *J. Chem. Phys.* **1987,** *87*, 5541-5553.

(54) Tomellini, M.; Fanfoni, M., Kinetics of Clustering on Surfaces. In *Interfacial Science - A chemistry for the 21st Century' Monograph*, Roberts, M. W., Ed. 1997; pp 129-161.

Entry for the Table of Contents